February 1, 2008

MSUHEP–050627

CITHE–68–2006

High–p_T Higgs Boson Production at Hadron Colliders to $\mathcal{O}(\alpha_s G_F^3)$

S. Mrenna[1]

Lauritsen Laboratory

California Institute of Technology

Pasadena, CA 91125

and

C.–P. Yuan[2]

Department of Physics and Astronomy

Michigan State University

East Lansing, MI 48824

Abstract

We study high–p_THiggs boson production at hadron colliders to order $\mathcal{O}(\alpha_s G_F^3)$ in hadron collisions. In particular, we investigate the process $g + q/\overline{q} \to q/\overline{q} + H$, where $q = u, d, c, s$, or b, for the LHC (a $\sqrt{s}$ =14 TeV, proton–proton collider). Our results are compared to the $\mathcal{O}(\alpha_s^3 G_F)$ calculation. The associated production of a high–p_T Higgs boson with a b–quark or anti–quark is comparable to the $\mathcal{O}(\alpha_s^3 G_F)$ calculation because of the large top quark mass and the additional contribution of electroweak gauge and Goldstone bosons. The associated production of light quarks, however, is not significant. We also comment on new physics effects in the framework of the electroweak chiral Lagrangian.

PAC codes: 12.15.Lk, 14.80.Bn

[1]mrenna@cithe502.cithep.caltech.edu

[2]yuan@msupa.pa.msu.edu

1 Introduction

With the discovery of the top quark [1], the only remaining element of the Standard Model (SM) particle spectrum is the Higgs boson. Experimentally, there are only lower bounds on M_H. LEP-I has placed the limit $M_H > 64.5$ GeV [2]. Theoretically, there are upper bounds in the SM from unitarity and triviality arguments [3]. One goal of the future High Energy Physics experimental program is to discover the Higgs boson and verify its properties or determine the alternative mechanism of electroweak symmetry breaking. The search for the Higgs boson at LEP-II is strictly limited by the available center of mass energy and luminosity, so that only $M_H < 90$–95 GeV can be probed for an energy of 190 GeV and 500 pb^{-1} of data [4]. The reach of a high–luminosity Tevatron collider is better, but becomes challenging above $M_H = 110$ GeV [5]. The LHC, on the other hand, is hoped to have enough energy, luminosity, and instrumentation to decisively probe the energy scale associated with electroweak symmetry breaking. This task is not as straight–forward as it may seem. One possible alternative to the SM is the Minimal Supersymmetric Standard Model (MSSM) with a constrained multi–dimensional parameter space [6, 7, 8]. The constrained MSSM models predict that the couplings of the lightest Higgs boson to SM particles is very SM–like, i.e. $\sin^2(\beta-\alpha) \simeq 1$, and its mass should be less than about 140 GeV [9]. In this case, to deduce supersymmetry, one must observe a superpartner directly or discern its presence in quantum corrections. Another alternative, a model with a strongly interacting scalar sector [10], predicts a greatly enhanced Higgs boson width even for a Higgs mass of a few hundred GeV, so that the Higgs boson signal can be hidden by backgrounds. Regardless of the scenario, a full verification of the properties of the Higgs boson requires a deep theoretical understanding of its properties. In this investigation, we concentrate on the high–$p_T$production of Higgs bosons, which is sensitive to loop corrections. The $\mathcal{O}(\alpha_s^3 G_F)$ contribution to high–p_THiggs boson production was calculated previously [11], where $G_F = (\sqrt{2}v^2)^{-1}$ and the vacuum expectation value $v = 246$ GeV. Here, we extend that calculation to include the $\mathcal{O}(\alpha_s G_F^3)$ contributions from electroweak gauge bosons, Goldstone bosons, and quarks. In particular, since the top mass is large, we expect to see an enhancement in the associated production of a Higgs boson with a b–quark or anti–quark in some kinematic region. We also expect this channel to be sensitive to the coupling of the electroweak gauge bosons and Goldstone bosons to the Higgs boson, since it does not vanish in the

limit that the $U(1)_Y$ and $SU(2)_L$ gauge couplings vanish.[3] We study this sensitivity in the framework of the electroweak chiral Lagrangian, which allows us to construct the most general effective Lagrangian that is consistent with $SU(2)_L \times U(1)_Y \to U(1)_{em}$ symmetry breaking. We show that with new physics, the $\mathcal{O}(\alpha_s G_F^3)$ contribution can be comparable to the $\mathcal{O}(\alpha_s^3 G_F)$ contribution for high–p_THiggs boson production. Another source of high–p_THiggs bosons is the $\mathcal{O}(\alpha_s G_F)$ tree level process. We show that this is small by examining the processes $q + \overline{q} \to b + \overline{b} + H$ and $g + g \to b + \overline{b} + H$. We also argue that any interference between this order amplitude and one of higher order is suppressed because the bottom quark mass m_b is much less than the electroweak symmetry breaking scale v.

2 High–$p_T$production of the Higgs boson to $\mathcal{O}(\alpha_s G_F^3)$

To $\mathcal{O}(\alpha_s G_F^3)$, the Higgs boson is produced at high–$p_T$from quark–gluon, antiquark–gluon, and quark–antiquark initial states. Since they are the most interesting, we will concentrate on the first two processes for the purpose of this discussion. The quark–antiquark annihilation process is typically an order of magnitude smaller at the LHC for $M_H \leq 400$ GeV. We chose to perform the calculation in the helicity formalism, since the amount of algebra is reduced significantly. Furthermore, we used the Feynman rules in the 't Hooft–Feynman gauge, since the electroweak gauge bosons and their associated Goldstone bosons have the same mass and, hence, loop integrals involving gauge bosons and Goldstone bosons have the same denominators. This choice is also advantageous for investigating the electroweak chiral Lagrangian.

We consider the process $g(p_g) + q(p_j) \to q(p_i) + H(p_H)$ to $\mathcal{O}(\alpha_s G_F^3)$, where the p_g and p_j are the four-momenta of the incoming particles and p_i and p_H are the four-momenta of the outgoing particles. The quark–antiquark initial state can be generated by the substitution $p_i \to -p_i, p_g \to -p_g$ and a reevaluation of the color factor. Contributions to the loop integral come from internal lines involving the weak isospin quark partner of q (we use the simplification $V_{ud} = V_{cs} = V_{tb} = 1$), gauge bosons, and Goldstone bosons. Some representative Feynman diagrams are illustrated in Figure 1. The amplitude for this process

[3]The $\mathcal{O}(\alpha_s^3 G_F)$ contribution does not depend on the electroweak gauge couplings, but is only sensitive to the coupling of the top quark to the Higgs boson.

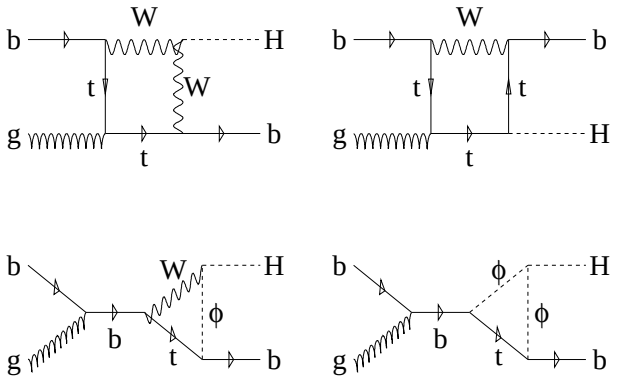

Figure 1: Some representative Feynman diagrams for the $\mathcal{O}(\alpha_s G_F^3)$ contributions to the process $g + b/\overline{b} \to b/\overline{b} + H$.

can be written as:

$$\mathcal{M}_{\lambda_i\lambda_j\lambda_g} \;=\; ig_s\overline{u}(\lambda_i,p_i)[\mathcal{F}\gamma_\mu + \mathcal{G}_\mu \not{p}_H]u(\lambda_j,p_j)\epsilon^\mu_{\lambda_g}, \tag{1}$$

where λ_i and λ_j are the fermion helicity indices, λ_g is the gluon polarization, γ_μ are 4×4 gamma matrices, $\not{a} = a^\mu\gamma_\mu$ for 4–vector a^μ, and equations of motion have been applied to the on–shell, 4–component spinors.

In addition, we have taken the limit $m_q \to 0$ for all q except t. The complex scalar $\mathcal{F}$ and the complex vector $\mathcal{G}_\mu$ are form factors resulting from the integration of the loop momentum, and their explicit expression are given in the Appendices I and II. The helicity amplitude can be re-written in terms of 2–component Weyl spinors using the bra–ket notation:[4]

$$\begin{aligned}
u_-(\lambda=-1/2,p_a) &= \omega_+^a|p_a-\rangle,\\
v_-(\lambda=+1/2,p_a) &= -\omega_+^a|p_a-\rangle,\\
u_+(\lambda=+1/2,p_a) &= \omega_+^a|p_a+\rangle,\\
v_+(\lambda=-1/2,p_a) &= -\omega_+^a|p_a+\rangle,
\end{aligned}$$

where $\omega_+^a = \sqrt{2E_a}$ for massless fermions with energy E_a, and $\langle p\pm| = (|p\pm\rangle)^\dagger$. These are the only components for massless fermions. For $p^\mu = (E, ps_\theta c_\phi, ps_\theta s_\phi, pc_\theta)$, where s_ψ and c_ψ are shorthand for $\sin\psi$ and $\cos\psi$, $|p+\rangle = (\cos\theta/2, e^{i\phi}\sin\theta/2)^{\rm T}$, and $|p-\rangle =$

[4] The 2–component Weyl spinors are defined by the relation $u_\pm = \frac{1}{2}(1\pm\gamma_5)u$, etc.

$(-e^{-i\phi}\sin\theta/2, \cos\theta/2)^{\mathrm{T}}$[5]. Also, the gluon polarization 4–vectors for left-handed (L) and right-handed (R) helicities can be written as:

$$\epsilon^{\mu}_{(L)} = \frac{e^{-i\phi}}{\sqrt{2}}[0, is_{\phi} + c_{\phi}c_{\theta}, -ic_{\phi} + s_{\phi}c_{\theta}, -s_{\theta}],$$
$$\epsilon^{\mu}_{(R)} = \frac{e^{i\phi}}{\sqrt{2}}[0, is_{\phi} - c_{\phi}c_{\theta}, -ic_{\phi} - s_{\phi}c_{\theta}, s_{\theta}],$$

where ϕ and θ are spherical coordinates of the gluon momentum. In the helicity basis, there are four non–vanishing amplitudes (as $m_q \to 0$). The parton–level cross section is:

$$d\hat{\sigma} = \frac{1}{F}\frac{1}{S}C_{gb}\sum_{\lambda_g=L,R}(|\mathcal{M}_{--\lambda_g}|^2 + |\mathcal{M}_{++\lambda_g}|^2)dR_2,$$
$$\mathcal{M}_{--\lambda_g} = ig_s\omega^i_+\omega^j_+\langle p_i - |[\mathcal{F}\gamma_{+\mu} + \mathcal{G}_{\mu}\not{p}_{H+}]|p_j-\rangle\epsilon^{\mu}_{\lambda_g},$$
$$\mathcal{M}_{++\lambda_g} = ig_s\omega^i_+\omega^j_+\langle p_i + |[\mathcal{F}\gamma_{-\mu} + \mathcal{G}_{\mu}\not{p}_{H-}]|p_j+\rangle\epsilon^{\mu}_{\lambda_g},$$

where the flux factor $F = 2\hat{s}$ for $\hat{s} = (p_g + p_j)^2$; the spin average factor $S = 2 \times 2$; the color factor is $C_{gq} = 4/(3 \times 8)$ for $g + q \to q + H$, and $C_{qq} = 4/(3 \times 3)$ for $q + \overline{q} \to g + H$; the gluon polarization is specified by λ_g; dR_s is the two–body phase space; $\gamma^{\mu}_{\pm}$ are the 2×2 matrices $(\mathbf{1}, \mp\sigma_i)$,[6] and $\not{a}_{\pm} = a_{\mu}\gamma^{\mu}_{\pm}$. In the above result, $\mathcal{M}_{++\lambda_g}$, which only contains contributions from Z^0–bosons, are small for two reasons. First, since we are only interested in initial and final states without t–quarks, the internal quark is always light (because of the neutral current) and has a tiny coupling to the Goldstone boson. Secondly, the left– and right–handed couplings of the Z^0–boson, which are smaller than the purely left–handed coupling of the $W^{\pm}$–bosons, appear in the squared matrix element to the fourth–power. For all practical purposes, then, the Z^0 contributions can be ignored, leaving only two independent helicity amplitudes, $\mathcal{M}_{--\lambda_g}$, differing only in the gluon polarization[7].

Because of gauge invariance, each amplitude satisfies the Ward Identity resulting from replacing the gluon polarization vector with the gluon four momentum. This simplifies to $\mathcal{F} + p_g \cdot \mathcal{G} = 0$. The form factors are calculated numerically using the FF Fortran library [12], so the Ward Identity can be verified numerically. Rotational and Lorentz invariance are also checked in the same manner.

The high–$p_T$production of the Higgs boson at a hadron collider is calculated by folding the parton–level cross section with the parton distribution functions (PDF). We use

[5] The superscript T denotes taking the transpose

[6] σ_i are Pauli matrices satisfying $\mathrm{Tr}(\sigma_i\sigma_j) = 2\delta_{ij}$.

[7] In our numerical results, we include all the contributions.

CTEQ2L parton distribution functions and evaluate coupling constants at the momentum scale $Q^2 = \hat{s}$. Unless otherwise stated, we use m_t=175 GeV in all calculations.

3 Numerical Results

High–p_THiggs boson production at a 2 TeV $\overline{\rm p}$p collider is too small to be observed for all practical purposes.[8] We present results only for the LHC (a 14 TeV pp collider). In Table I, we list the production cross section to $\mathcal{O}(\alpha_s G_F^3)$ for several Higgs boson masses as well as the $\mathcal{O}(\alpha_s^3 G_F)$ contribution for the transverse momentum of the Higgs boson $p_T^H > 30$ GeV. There are separate columns for the associated production of the Higgs boson with b–quarks and u, d, s, c–quarks. For all of these results, we include both the quark and antiquark contribution. For the associated production of H with a b–quark or anti–quark, the total $\mathcal{O}(\alpha_s G_F^3)$ cross section for $p_T^H > 30$ GeV is as large as 10–20% of the $\mathcal{O}(\alpha_s^3 G_F)$ for $M_H = 100 - 200\,\text{GeV}$. As the transverse momentum of the Higgs boson increases, the $\mathcal{O}(\alpha_s G_F^3)$ contribution becomes relatively more important. For this process, the m_t dependence is minimal. For instance, for $M_H = 110\,\text{GeV}$, the total $\mathcal{O}(\alpha_s G_F^3)$ cross section of $b/\overline{b}+H$ is 16.9 fb and 17.5 fb for $m_t = 160\,\text{GeV}$ and 190 GeV, respectively. For the associated production of H with light quark, the $\mathcal{O}(\alpha_s G_F^3)$ cross section for $p_T^H > 30$ GeV is never more than about 3% of the $\mathcal{O}(\alpha_s^3 G_F)$ for $M_H = 100 - 200\,\text{GeV}$. The cross section for $q + \overline{q} \to H + g$ is much smaller than for the corresponding process $g + q/\overline{q} \to q/\overline{q} + H$, having values (1.5,.15) fb for $M_H = (110{,}400)\,\text{GeV}$, and will not be discussed further.

We also studied the p_T^H dependence of the cross section as a function of M_H. In Figure 2 we show the cross section integrated above p_T^H for $b/\overline{b} + H$ production to $\mathcal{O}(\alpha_s G_F^3)$ and $\mathcal{O}(\alpha_s^3 G_F)$ in the same M_H range as in Table I. The mean p_T^H of the $\mathcal{O}(\alpha_s G_F^3)$ process, for p_T^H in the range 50–350 GeV, is a slowly varying function of M_H below $M_H = 180$ GeV, with a value of approximately 120 GeV. Above $M_H = 180$ GeV, the mean p_T^H ranges takes on the values (139,152) GeV for $M_H = (200{,}400)$ GeV. The mean p_T^H of the $\mathcal{O}(\alpha_s^3 G_F)$ process is strongly dependent on the lower transverse momentum cutoff needed to regulate the $p_T^H \to 0$ divergence associated with the gluon progagator, and is somewhat smaller than that for the $\mathcal{O}(\alpha_s G_F^3)$ process.

Finally, we address the issue of the $\mathcal{O}(\alpha_s G_F)$ process $g + b/\overline{b} \to b/\overline{b} + H$, which is a tree

[8] The rate at 2 TeV ($\overline{\rm p}$p) is about two orders of magnitude smaller than that at 14 TeV (pp).

Higgs Production, $p_T^H > 30$ GeV, $m_t = 175$ GeV				
M_H	$\sigma(g + b/\overline{b} \to b/\overline{b} + H)$ (fb)		$\sigma(g + q/\overline{q} \to q/\overline{q} + H)$ (fb)	
(GeV)	$\mathcal{O}(\alpha_s G_F^3)$	$\mathcal{O}(\alpha_s^3 G_F)$	$\mathcal{O}(\alpha_s G_F^3)$	$\mathcal{O}(\alpha_s^3 G_F)$
110	17.1	125.4	46.5	2.2×10^3
140	15.1	88.8	37.0	1.6×10^3
180	7.4	61.6	25.2	1.2×10^3
400	1.9	29.6	0.5	0.7×10^3

Table 1: Cross section for Higgs boson production at high–p_T.

level process. To estimate the size of this cross section, we used the processes $q+\overline{q} \to b+\overline{b}+H$ and $g + g \to b + \overline{b} + H$ in Pythia 5.7 [13] with $p_T^H > 50$ GeV. We obtained the values (4.5,3.0,2.0,.3) fb for M_H = (110,140,180,400) GeV. In the limit that $m_b \to 0$, there is no interference between the tree level process and the higher order amplitudes[9], so any observed cross section is primarily the $\mathcal{O}(\alpha_s^3 G_F)$ and $\mathcal{O}(\alpha_s G_F^3)$ processes.

In summary, we find that to accurately predict the cross section and test the properties of an intermediate mass Higgs boson produced at high–p_T in association with b quarks and anti–quarks, the $\mathcal{O}(\alpha_s G_F^3)$ contributions should be included with the $\mathcal{O}(\alpha_s^3 G_F)$ contributions. Because of the large top quark masss, the $\mathcal{O}(\alpha_s G_F^3)$ contributions are larger than the tree-level contributions of $\mathcal{O}(\alpha_s G_F)$ for large p_T^H. Although the production rate of $\mathcal{O}(\alpha_s G_F^3)$ for the associated production of the Higgs boson with a light quark or anti–quark is not negligible, it is only a few percent of the $\mathcal{O}(\alpha_s^3 G_F)$ rate, and therefore is probably not distinguishable from the uncertainty in the PDF.

4 The Electroweak Chiral Lagrangian and Non-Standard Model Couplings

The process under consideration is sensitive to electroweak symmetry breaking in three different sets of couplings. First, there is the t-b-W vertex. The additional non-standard couplings can be deduced from the chiral Lagrangian [14]:

$$\mathcal{L} \;=\; -\sqrt{2}\kappa_L^{CC}\overline{t_L}\gamma^\mu b_L \Sigma_\mu^+ - \sqrt{2}\kappa_L^{CC\dagger}\overline{b_L}\gamma^\mu t_L \Sigma_\mu^-$$

[9] We note that the tree level amplitude and the higher order amplitudes have different helicity structure in the $m_b \to 0$ limit.

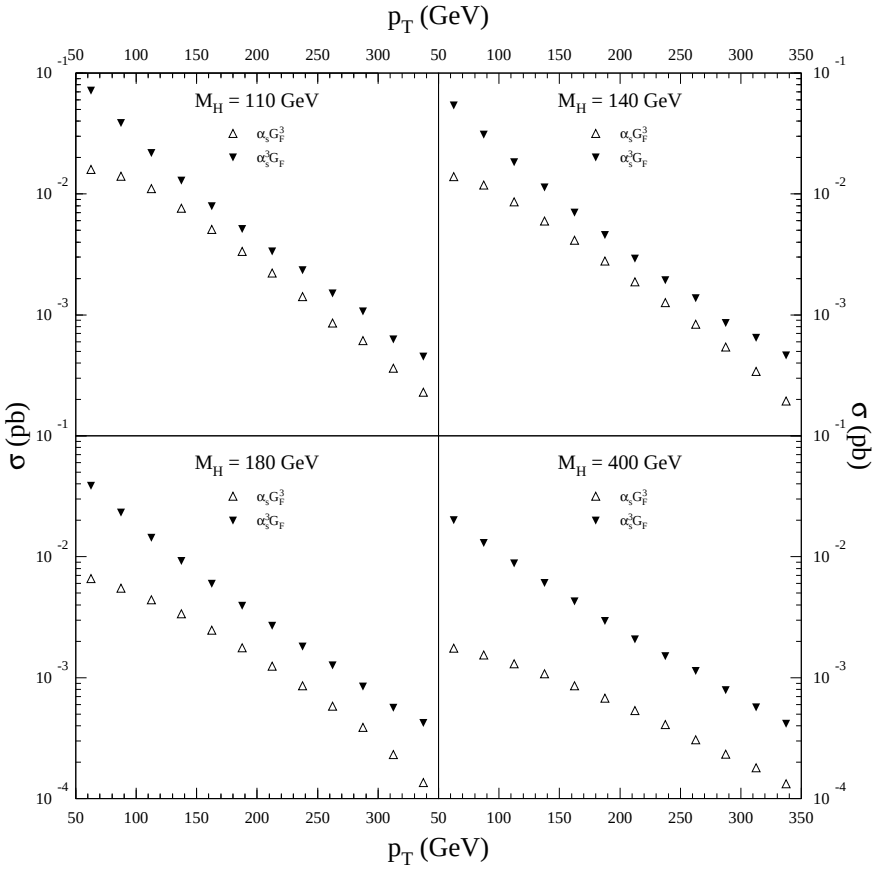

Figure 2: The cross section integrated above p_T^H for $b/\overline{b} + H$ production to $\mathcal{O}(\alpha_s G_F^3)$ and $\mathcal{O}(\alpha_s^3 G_F)$ for various M_H.

$$-\sqrt{2}\kappa_R^{CC}\overline{t_R}\gamma^\mu b_R\Sigma_\mu^+ - \sqrt{2}\kappa_R^{CC\dagger}\overline{b_R}\gamma^\mu t_R\Sigma_\mu^-, \tag{2}$$

where $\Sigma_\mu^\pm = \frac{1}{\sqrt{2}}(\Sigma_\mu^1 \mp i\Sigma_\mu^2)$ for $\Sigma_\mu^a = -\frac{i}{2}\mathrm{Tr}(\sigma^a\Sigma^\dagger D_\mu\Sigma)$, and the action of the covariant derivative is $D_\mu\Sigma = \partial_\mu\Sigma - igW_\mu^a\frac{\sigma^a}{2}\Sigma + ig'\Sigma B_\mu\frac{\sigma^3}{2}$. The matrix field $\Sigma = \exp\left(i\frac{\phi^a\sigma^a}{v}\right)$, where σ^a, $a = 1, 2, 3$, are the Pauli matrices, and ϕ^a's are the Goldstone bosons. Second, there is the Yukawa coupling between the Higgs boson and top quark. The most general Yukawa coupling of the fermion doublet F in the chiral Lagrangian is:

$$\mathcal{L} = -\frac{c_0}{v}H\overline{F}MF, \tag{3}$$

where M is a 2×2 mass matrix. In the Standard Model, $c_0 = 1$. Third, the coupling of the Higgs boson and the electroweak Goldstone bosons comes from the Lagrangian:

$$\begin{aligned}\mathcal{L} &= \frac{1}{2}\partial_\mu H\partial^\mu H - \frac{1}{2}M_H^2H^2 - V(H) \\ &\quad +(\frac{c_1}{2}vH + \frac{c_2}{4}H^2)\mathrm{Tr}\left(D_\mu\Sigma^\dagger D^\mu\Sigma\right).\end{aligned} \tag{4}$$

In the Standard Model, $c_1 = c_2 = 1$.

To illustrate that new physics effects may enhance the $\mathcal{O}(\alpha_s G_F^3)$ rate but not the $\mathcal{O}(\alpha_s^3 G_F)$ rate, we study the effects of new physics arising from the scalar sector of the Lagrangian, as shown in Eq.(4). In this case, the $\mathcal{O}(\alpha_s^3 G_F)$ contribution is not modified. As shown in Ref. [10], some models of the symmetry breaking sector allow the coefficient c_1 in Eq.(4) to be larger than 1. (c_2 is irrelevant to the processes of interest.) For instance, $c_1 = \sqrt{8/3}$ was discussed in Ref. [10]. Because new physics can simutaneously modify the interactions of t-b-W and W-W-H, we do not intend to give predictions for any specific model. For simplicity, we only study the effects of new physics due to c_1 in the limit that the $SU(2)_L \times U(1)_Y$ gauge couplings g and g' vanish. Table II contains some of our results.

Although these rates do not represent the true rates of the process $g + b/\overline{b} \to b/\overline{b} + H$, they illustrate that the rates can vary by about a factor of 2 for a heavier Higgs boson. If the electroweak corrections to high–p_T Higgs production are substantially modified by new physics at the order $\mathcal{O}(\alpha_s G_F^3)$, then this can be observed in $b/\overline{b} + H$ production at future hadron colliders.

5 Discussion and Conclusions

Because the top quark mass is large, of the order of v, the interaction of the top quark and the Goldstone bosons is strong and, therefore, can be sensitive to the electroweak

Higgs + $b/\overline{b}$ Rate (fb) as $g, g' \to 0$ $p_T^H >$ 30 GeV, m_t = 175 GeV					
M_H	Chiral Lagrangian coefficient c_1				
(GeV)	$-.5$	0.0	0.5	1.0	1.5
110	1.09	0.87	0.78	0.83	1.01
140	1.26	0.79	0.87	1.49	2.64
180	0.74	0.69	2.00	4.67	8.71
200	0.42	0.63	1.76	3.82	6.81
250	0.19	0.49	1.32	2.70	4.60
300	0.12	0.36	1.00	2.01	3.41
400	0.06	0.21	0.59	1.20	2.03

Table 2: Effects of new physics on high-p_THiggs boson production as $g, g' \to 0$. In the Standard Model, $c_1 = 1$.

symmetry breaking sector. For the associated production of $b/\overline{b}$ with the Higgs boson at high p_T, the SM electroweak corrections of $\mathcal{O}(\alpha_s G_F^3)$, involving the large top quark mass, is comparable to the the QCD corrections of $\mathcal{O}(\alpha_s^3 G_F)$. On the other hand, the associated production of light quarks and anti–quarks with the Higgs boson is not significant because no large fermion mass is involved.

Once the Higgs boson is discovered, it is important to test whether it is a Standard Model Higgs boson or some other non-standard scalar particle. The cross section of the Higgs boson production at large transverse momentum can be sensitive to new physics which modify either t-b-W, t-t-H, or W-W-H vertices. Among them, only the t-t-H vertex can modify the $\mathcal{O}(\alpha_s^3 G_F)$ contributions. In contrast, all of them can modify the $\mathcal{O}(\alpha_s G_F^3)$ contributions. As illustrated in Table II, it is possible that the $\mathcal{O}(\alpha_s G_F^3)$ rate is enhanced by more than a factor of 2 due to new physics effects. Therefore, $\mathcal{O}(\alpha_s G_F^3)$ contributions should also be included when testing SM predictions.

Acknowledgments

C.-P.Y. thanks A. Abbasabadi, D. Bower-Chao, and W. Repko for useful discussions. S.M. was supported in part by DOE grant DE–FG03–92–ER40701. The work of C.P.Y. was

supported in part by NSF grant No. PHY-9309902.

Appendix I: Loop Integration

In calculating the helicity amplitudes, one must evaluate loop integrals of the form

$$X \equiv \frac{1}{i\pi^2}\int \frac{d^nQ\{1, Q^\mu, Q^\mu Q^\nu\}}{(Q^2-m_1^2)((Q+P)^2-m_2^2)\cdots}.$$

For triangle diagrams, $X = C$, and for box diagrams, $X = D$.

Triangle Diagrams

The scalar function for triangle diagrams, showing explicitly its dependent variables, is:

$$C_0(m_1^2, m_2^2, m_3^2, p_1^2, p_2^2, p_3^2) = \frac{1}{i\pi^2}\int \frac{d^nQ}{(Q^2-m_1^2)[(Q+p_1)^2-m_2^2][(Q+p_1+p_2)^2-m_3^2]},$$

where the internal line masses m_i are labelled by the external lines, p_1 is the momentum flowing between the lines with masses m_1 and m_2, p_2 between m_2 and m_3, and $p_3 = -p_1 - p_2$ between m_3 and m_1. The vector integral over Q^μ is

$$C_{11}p_1^\mu + C_{12}p_2^\mu.$$

Similary, the tensor integral over $Q^\mu Q^\nu$ is

$$C_{21}p_1^\mu p_1^\nu + C_{22}p_2^\mu p_2^\nu + C_{23}\{p_1^\mu p_2^\nu + p_1^\nu p_2^\mu\} + C_{24}g^{\mu\nu}.$$

Box Diagrams

The scalar function for box diagrams, similar to the triangle diagrams, can be written as $D_0(m_1^2, m_2^2, m_3^2, m_4^2, p_1^2, p_2^2, p_3^2, p_4^2, (p_1+p_2)^2, (p_2+p_3)^2)$. The notation is an obvious generalization of that for the triangle diagrams. The vector integral over Q^μ is

$$D_{11}p_1^\mu + D_{12}p_2^\mu + D_{13}p_3^\mu.$$

The tensor integral over $Q^\mu Q^\nu$ is

$$D_{21}p_1^\mu p_1^\nu + D_{22}p_2^\mu p_2^\nu + D_{23}p_3^\mu p_3^\nu +$$
$$D_{24}\{p_1^\mu p_2^\nu + p_1^\nu p_2^\mu\} + D_{25}\{p_1^\mu p_3^\nu + p_1^\nu p_3^\mu\} + D_{26}\{p_2^\mu p_3^\nu + p_2^\nu p_3^\mu\} + D_{27}g^{\mu\nu}.$$

Appendix II: Form Factors

In 't Hooft-Feynman gauge, there are 20 Feynman diagrams containing $W^{\pm}$–bosons and $\phi^{\pm}$ Goldstone bosons involved in the process $g + b/\overline{b} \to b/\overline{b} + H$ at $\mathcal{O}(\alpha_s G_F^3)$ for $m_b = 0$. As discussed in the text, the 3 diagrams involving Z^0–bosons and ϕ^0 Goldstone bosons are negligible. Some typical diagrams are shown in Figure 1. In this appendix, we list the individual contributions to the form factors [cf. Eq.(1)] from each Feynman diagram for the process $g(q_g) + b(q_3) \to b(q_1) + H(q_2)$. All momenta are defined pointing *in* to the Feynman diagram, i.e. the outgoing quark (q_1) and Higgs boson (q_2) four momenta have a negative energy component. There are 12 triangle diagrams, with terms labelled $\mathcal{F}_9 - \mathcal{F}_{20}$, and 8 box diagrams, with terms $\mathcal{F}_1 - \mathcal{F}_8$ and $\mathcal{G}_1^{\mu} - \mathcal{G}_8^{\mu}$. The full form factors are $\mathcal{F} = \sum_{i=1}^{20} \mathcal{F}_i$ and $\mathcal{G}^{\mu} = \sum_{i=1}^{8} \mathcal{G}_i^{\mu}$. The following expressions contain the invariant masses $s_{ij} = (q_i + q_j)^2$ and $s = (q_1 + q_2 + q_3)^2 = q_g^2$. We have used the relation $M_W = \frac{1}{2} g v$ to re–express the electroweak coupling constants in terms of masses and the vacuum expectation value v. The process involving light quarks in the initial and final state can be deduced by setting $m_t = 0$. The limit $g, g' \to 0$, which we take to study the electroweak chiral Lagrangian, is obtained by eliminating all terms with an explicit M_W dependence. All triangle diagrams contain progagators for one fermion and two gauge or Goldstone bosons. The box diagrams fall into two categories, those containing two fermion and two gauge or Goldstone boson propagators (denoted *t-t-W-W*) and those containing three fermion and one gauge or Goldstone boson propagators (denoted *t-t-t-W*).

Triangle Diagrams

$$
\begin{aligned}
\mathcal{F}_9 &= -8 C_{12} M_W^4 / v^3 \\
\mathcal{F}_{10} &= -2 C_{12} m_t^2 M_H^2 / v^3 \\
\mathcal{F}_{11} &= 2 m_t^2 M_W^2 (-2 C_{00} - C_{12}) / v^3 \\
\mathcal{F}_{12} &= -2 m_t^2 M_W^2 (-C_{00} + C_{12}) / v^3 \\
\mathcal{F}_{13} &= -8 C_{12} M_W^4 / v^3 \\
\mathcal{F}_{14} &= -2 C_{12} m_t^2 M_H^2 / v^3 \\
\mathcal{F}_{15} &= 2 m_t^2 M_W^2 (C_{00} - C_{12}) / v^3 \\
\mathcal{F}_{16} &= -2 m_t^2 M_W^2 (2 C_{00} + C_{12}) / v^3
\end{aligned}
$$

$$
\begin{aligned}
\mathcal{F}_{17} &= 2m_t^2 M_W^2(-2C_{00} - 4C_{11})/v^3 \\
\mathcal{F}_{18} &= 2m_t^4(-C_{00} - 2C_{11})/v^3 \\
\mathcal{F}_{19} &= 2m_t^2 M_W^2(-2C_{00} - 4C_{11})/v^3 \\
\mathcal{F}_{20} &= 2m_t^4(-C_{00} - 2C_{11})/v^3
\end{aligned}
$$

Note that there are no tensor contributions from the triangle diagrams, i.e. no C_{2i}.

Box Diagrams

t-t-W-W diagrams

$$
\begin{aligned}
\mathcal{F}_1 &= -8M_W^4(2D_{27} - D_{00}m_t^2 + (D_{22} - D_{24} + D_{25} - D_{26})M_H^2 \\
&\quad +(D_{11} + D_{25})s + (D_{24} - D_{25})s_{12} - (D_{11} + D_{12} - D_{25} + D_{26})s_{23})/v^3 \\
\mathcal{F}_2 &= -2m_t^2 M_H^2(2D_{27} - D_{00}m_t^2 + (D_{22} - D_{24} + D_{25} - D_{26})M_H^2 + \\
&\quad (D_{13} + D_{25})s + (D_{12} - D_{13} + D_{24} - D_{25})s_{12} - (D_{25} - D_{26})s_{23})/v^3 \\
\mathcal{F}_3 &= -2m_t^2 M_W^2(-2D_{27} + D_{13}s + (2D_{00} + D_{12} - D_{13})s_{12})/v^3 \\
\mathcal{F}_4 &= 2m_t^2 M_W^2(2D_{27} + (D_{00} + D_{11})s + (-2D_{00} - D_{11} + D_{12})s_{23})/v^3 \\
\mathcal{G}_1^\mu &= -16M_W^4((-D_{11} - D_{24})q_1^\mu + (-D_{12} - D_{22})q_2^\mu + (-D_{12} - D_{26})q_3^\mu)/v^3 \\
\mathcal{G}_2^\mu &= -4m_t^2 M_H^2((-D_{12} - D_{24})q_1^\mu + (-D_{12} - D_{22})q_2^\mu + (-D_{13} - D_{26})q_3^\mu)/v^3 \\
\mathcal{G}_3^\mu &= -4m_t^2 M_W^2((-2D_{00} - 2D_{11} - D_{12} - D_{24})q_1^\mu \\
&\quad +(-2D_{00} - 3D_{12} - D_{22})q_2^\mu + (-3D_{13} - D_{26})q_3^\mu)/v^3 \\
\mathcal{G}_4^\mu &= 4m_t^2 M_W^2((-2D_{00} - 2D_{11} + D_{12} + D_{24})q_1^\mu \\
&\quad +(-D_{12} + D_{22})q_2^\mu + (-D_{13} + D_{26})q_3^\mu)/v^3
\end{aligned}
$$

t-t-t-W diagrams

$$
\begin{aligned}
\mathcal{F}_5 &= 4m_t^2 M_W^2(D_{00}m_t^2 + (-D_{22} + D_{24} - D_{25} + D_{26})M_H^2 - (2D_{11} + D_{25})s \\
&\quad +(-D_{24} + D_{25})s_{12} + (-D_{00} + 2D_{11} - 2D_{12} + D_{25} - D_{26})s_{23})/v^3 \\
\mathcal{F}_6 &= 2m_t^4(D_{00}m_t^2 + (-D_{22} + D_{24} - D_{25} + D_{26})M_H^2 - (2D_{13}s + D_{25})s \\
&\quad +(-D_{00} - 2D_{12} + 2D_{13} - D_{24} + D_{25})s_{12} + (D_{25} - D_{26})s_{23})/v^3 \\
\mathcal{F}_7 &= 4m_t^2 M_W^2(D_{00}m_t^2 + (-D_{22} + D_{24} - D_{25} + D_{26})M_H^2 \\
&\quad +(D_{00} - D_{11} + D_{13} - D_{25})s + (-D_{00} + D_{12} - D_{13} - D_{24} + D_{25})s_{12} \\
&\quad +(D_{11} - D_{12} + D_{25} - D_{26})s_{23})/v^3
\end{aligned}
$$

$$
\begin{aligned}
\mathcal{F}_8 &= 2m_t^4(D_{00}m_t^2 + (-D_{22} + D_{24} - D_{25} + D_{26})M_H^2 \\
&\quad +(D_{00} + D_{11} - D_{13} - D_{25})s + (-D_{12} + D_{13} - D_{24} + D_{25})s_{12} \\
&\quad +(-D_{00} - D_{11} + D_{12} + D_{25} - D_{26})s_{23})/v^3 \\
\mathcal{G}_5^\mu &= 8m_t^2 M_W^2((3D_{11} + 2D_{24})q_1^\mu + (D_{00} + 3D_{12} + 2D_{22})q_2^\mu \\
&\quad +(D_{00} + 2D_{12} + D_{13} + 2D_{26})q_3^\mu)/v^3 \\
\mathcal{G}_6^\mu &= 4m_t^4((D_{00} + D_{11} + 2D_{12} + 2D_{24})q_1^\mu + (D_{00} + 3D_{12} + 2D_{22})q_2^\mu \\
&\quad +(3D_{13} + 2D_{26})q_3^\mu)/v^3 \\
\mathcal{G}_7^\mu &= 8m_t^2 M_W^2((D_{11} + 2D_{24})q_1^\mu + (D_{12} + 2D_{22})q_2^\mu \\
&\quad +(-D_{00} + 2D_{12} - D_{13} + 2D_{26})q_3^\mu)/v^3 \\
\mathcal{G}_8^\mu &= 4m_t^4((-D_{00} - D_{11} + 2D_{12} + 2D_{24})q_1^\mu + (D_{12} + 2D_{22})q_2^\mu \\
&\quad +(D_{13} + 2D_{26})q_3^\mu)/v^3
\end{aligned}
$$

References

[1] F. Abe *et al.*, Phys. Rev. Lett. **73**, 225 (1994);
S. Abachi *et al.*, Phys. Rev. Lett. **72**, 2138 (1994).

[2] P. Darriulat, conference summary of the 27th International Conference on High Energy Physics, Glasgow, 1994 (unpublished).

[3] J.F. Gunion, H.E. Haber, G.L. Kane, S. Dawson, **The Higgs Hunter's Guide**, Addison–Wesley, 1990.

[4] P. Giacomelli, CERN-PPE-93-18, 2nd Trieste Conference on Recent Development in the Phenomenology of Particle Physics (1993).

[5] A. Stange, W. Marciano, and S. Willenbrock, Phys. Rev. **D49** (1994) 1354;
J.F. Gunion and T. Han, Phys. Rev. **D51** (1995) 1051;
S. Mrenna and G.L. Kane, hep-ph/9406337, 1994.

[6] R. Arnowitt and P. Nath, Phys. Rev. Lett. **70** (1993) 3696.

[7] J.L. Lopez, D.V. Nanopoulos, H. Pois, X. Wang, and A. Zichichi, Phys. Lett. **B306** (1993) 73.

[8] G.L. Kane, C. Kolda, L. Roszkowski, and J.D. Wells, Phys. Rev. **D49** (1994) 6173.

[9] G.L. Kane, C. Kolda and J.D. Wells, Phys. Lett. **70** (1993) 2686.

[10] R. Chivukula, M. Dugan, and M. Golden, Phys. Lett. **B336** (1994) 62.

[11] R.K. Ellis, I. Hinchliffe, M. Soldate, and J.J. van der Bij, Nucl. Phys. **B297** (1988) 221.

[12] G.J. van Oldenborgh, "FF, A Package to Evaluate One–Loop Feynman Diagrams", NIKHEF–H/90–15, (1990).

[13] H.U. Bengtsson and T. Sjöstrand, Computer Physics Commun. **43** (1987) 43.

[14] E. Malkawi and C.–P. Yuan, Phys. Rev. **D50** (1994) 4462;
C.-P. Yuan, "Top Quark Physics," to appear in the proceedings of the VIth Mexican School of Particles and Fields, Villahermosa, Mexico, 3–7 October, 1994.